JACS
JOURNAL OF THE AMERICAN CHEMICAL SOCIETY
Article
pubs.acs.org/JACS

High-Performance Ternary Organic Solar Cell Enabled by a Thick Active Layer Containing a Liquid Crystalline Small Molecule Donor

Guichuan Zhang,[†] Kai Zhang,[†] Qingwu Yin,[†] Xiao-Fang Jiang,[†] Zaiyu Wang,[‡] Jingming Xin,[‡] Wei Ma,[‡] He Yan,[⊥] Fei Huang,*[,†] and Yong Cao[†]

[†]Institute of Polymer Optoelectronic Materials and Devices, State Key Laboratory of Luminescent Materials and Devices, South China University of Technology, Guangzhou 510640, P. R. China

[‡]State Key Laboratory for Mechanical Behavior of Materials, Xi'an Jiaotong University, Xi'an 710049, P. R. China

[⊥]Department of Chemistry and Hong Kong Branch of Chinese National Engineering Research Center for Tissue Restoration and Reconstruction, Hong Kong University of Science and Technology, Clear Water Bay, Kowloon, Hong Kong 999077, P. R. China

Supporting Information

ABSTRACT: Ternary organic solar cells (OSCs) have attracted much research attention in the past few years, as ternary organic blends can broaden the absorption range of OSCs without the use of complicated tandem cell structures. Despite their broadened absorption range, the light harvesting capability of ternary OSCs is still limited because most ternary OSCs use thin active layers of about 100 nm in thickness, which is not sufficient to absorb all photons in their spectral range and may also cause problems for future roll-to-roll mass production that requires thick active layers. In this paper, we report a highly efficient ternary OSC (11.40%) obtained by incorporating a nematic liquid crystalline small molecule (named benzodithiophene terthiophene rhodanine (BTR)) into a state-of-the-art PTB7-Th:PC71BM binary system. The addition of BTR into PTB7-Th:PC71BM was found to improve the morphology of the blend film with decreased $\pi-\pi$ stacking distance, enlarged coherence length, and enhanced domain purity. This resulted in more efficient charge separation, faster charge transport, and less bimolecular recombination, which, when combined, led to better device performance even with thick active layers. Our results show that the introduction of highly crystalline small molecule donors into ternary OSCs is an effective means to enhance the charge transport and thus increase the active layer thickness of ternary OSCs to make them more suitable for roll-to-roll production than previous thinner devices.

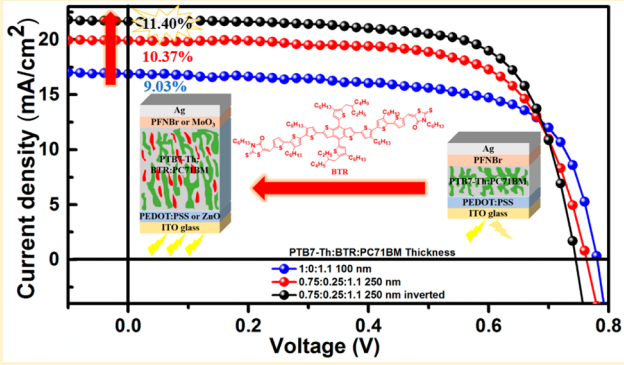

INTRODUCTION

Bulk heterojunction (BHJ) organic solar cells (OSCs) with donor/acceptor bicontinuous interpenetrating networks have drawn much research attention due to their advantages in achieving lightweight, flexible, and low-cost devices.[1−5] Over the past two decades, tremendous efforts have been made to improve the power conversion efficiency (PCE) of OSCs via the design of new donor[6−11] and acceptor[12−16] materials, interface engineering,[17−20] new processing methods,[21,22] and innovative device architectures.[23−26] The OSC community recently developed a new type of ternary OSC that was designed to collect both high- and low- energy photons by using three components in a single active layer.[27−30] Because of rapidly improving efficiencies of ternary OSCs, an increasing amount of research effort has been directed toward these OSCs. Many efficient ternary systems have been reported that have improved the PCE to more than 10%, owing to various factors such as alignment of the cascade energy level,[31−33] the formation of alloys,[34−36] improvement of morphology,[37−40] and increased mobility.[41,42]

However, current ternary OSCs are still quite limited in their absorption strength (despite the broadened absorption) because nearly all ternary OSCs have active layers of about 100 nm in thickness, which is not thick enough to absorb all photons in the absorption range of the cell. For this reason, the short-circuit current density (J_{SC}) of current ternary OSCs is not fully optimized,[31,34,42,43] and roll-to-roll mass production of such thin-film devices is also difficult.[11,44−49] It has been theoretically predicted by Ratner et al. that thick-film ternary OSCs will obtain higher PCEs than thin-film devices and can achieve a PCE up to 14%.[50] Therefore, it is important to increase the thickness of the ternary active layer without sacrificing any device parameters such as the fill factor (FF).

Received: November 21, 2016
Published: January 27, 2017

DOI: 10.1021/jacs.6b11991
J. Am. Chem. Soc. 2017, 139, 2387−2395

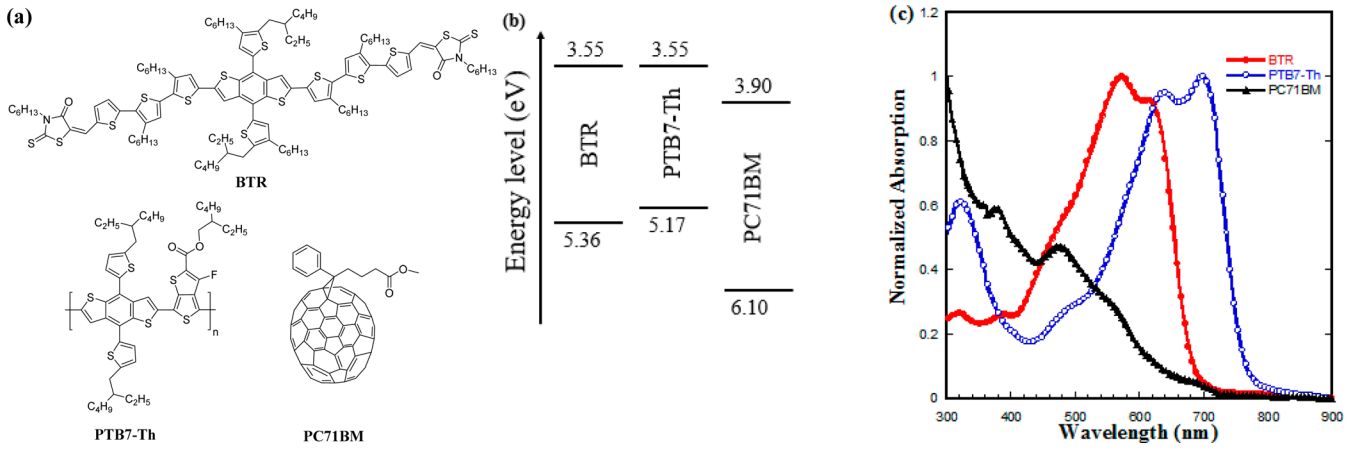

Figure 1. (a) Chemical structures, (b) energy levels diagram, and (c) normalized absorption spectra of PTB7-Th, BTR, and PC71BM.

Table 1. Photovoltaic Performances of OSCs Using Various Ratios of PTB7-Th:BTR:PC71BM Thin Active Layers Under AM 1.5G Irradiation (100 mW cm^{-2})

PTB7-Th:BTR:$PC_{71}BM$	thickness [nm]	V_{OC}[V]	J_{SC} (J_{calcd})[b] [mA cm^{-2}]	FF [%]	PCE[a] [%]	PCE_{bset} [%]
1:0:1.1	100	0.782 ± 0.009	16.8 ± 0.1 (15.96)	68.0 ± 0.4	8.9 ± 0.1	9.03
0.9:0.1:1.1	100	0.784 ± 0.002	17.2 ± 0.2 (16.47)	73.2 ± 0.5	9.9 ± 0.1	10.09
0.8:0.2:1.1	100	0.783 ± 0.002	17.1 ± 0.1 (16.47)	75.3 ± 0.6	10.1 ± 0.1	10.15
0.75:0.25:1.1	100	0.782 ± 0.001	17.1 ± 0.2 (16.50)	75.7 ± 0.7	10.1 ± 0.1	10.16
0.7:0.3:1.1	100	0.775 ± 0.001	16.8 ± 0.1 (15.95)	74.6 ± 0.4	9.7 ± 0.01	9.75
0:1:1.1	110	0.886 ± 0.007	10.5 ± 0.2 (9.89)	73.6 ± 0.7	6.8 ± 0.2	6.97

[a]Statistical data obtained from 10 independent devices. [b]The J_{SC} calculated from the EQE spectrum.

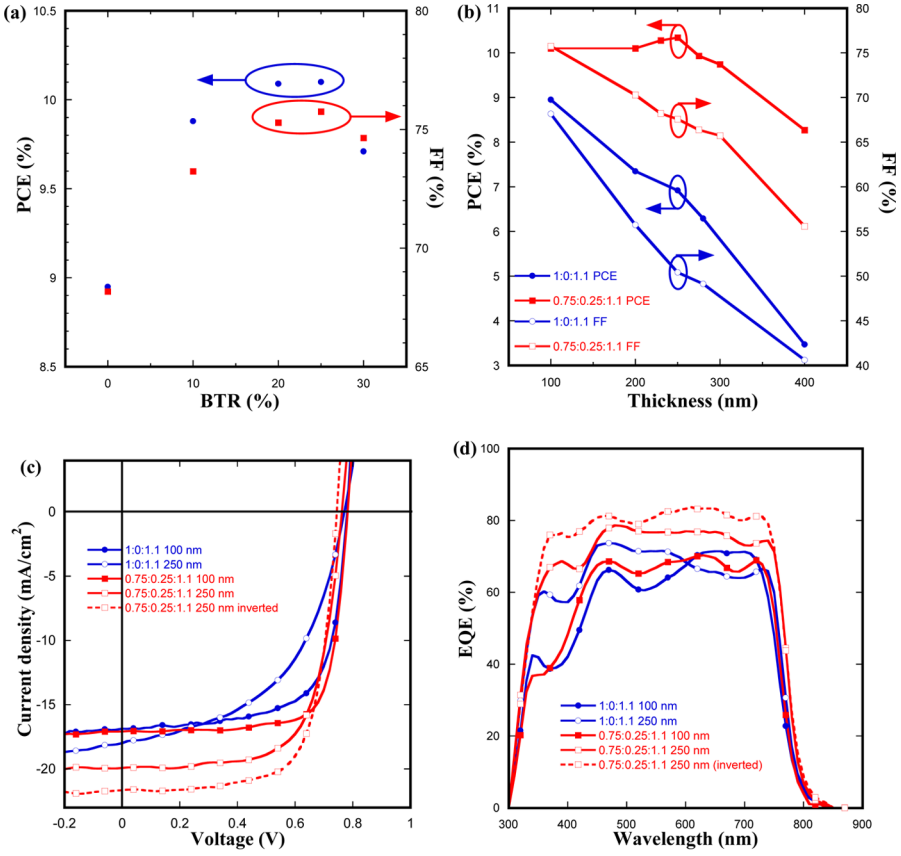

Figure 2. (a) PCE and FF of OSCs with thin active layer versus various contents of BTR. (b) PCE and FF of OSCs with PTB7-Th:BTR:PC71BM ratios of 1:0:1.1 and 0.75:0.25:1.1 versus active layer thickness. (c) *J*–*V* and (d) EQE curves of OSCs with PTB7-Th:BTR:PC71BM ratios of 1:0:1.1 and 0.75:0.25:1.1 with thin and thick active layers.

DOI: 10.1021/jacs.6b11991
J. Am. Chem. Soc. 2017, 139, 2387–2395

Table 2. Photovoltaic Performance of OSCs Using Various Ratios of PTB7-Th:BTR:PC71BM Thick Active Layers Under AM 1.5G Irradiation (100 mW cm^{-2})

PTB7-Th:BTR:$PC_{71}BM$	thickness [nm]	V_{OC} [V]	J_{SC} (J_{calcd})[b] [mA cm^{-2}]	FF [%]	PCE[a] [%]	PCE_{bset} [%]
1:0:1.1	200	0.774 ± 0.001	17.0 ± 0.1	55.7 ± 1.0	7.4 ± 0.1	7.45
1:0:1.1	250	0.771 ± 0.002	17.8 ± 0.2 (17.06)	50.6 ± 0.9	6.9 ± 0.1	7.07
1:0:1.1	280	0.765 ± 0.002	16.7 ± 0.3	49.1 ± 0.8	6.3 ± 0.2	6.50
1:0:1.1	400	0.757 ± 0.010	11.3 ± 1.2	40.7 ± 0.8	3.5 ± 0.5	4.03
0.75:0.25:1.1	200	0.766 ± 0.002	18.8 ± 0.2	70.3 ± 0.2	10.1 ± 0.1	10.19
0.75:0.25:1.1	230	0.759 ± 0.002	19.8 ± 0.1	68.3 ± 0.5	10.2 ± 0.1	10.34
0.75:0.25:1.1	250	0.763 ± 0.001	20.0 ± 0.2 (19.12)	67.4 ± 0.6	10.3 ± 0.1	10.37
0.75:0.25:1.1	275	0.761 ± 0.002	19.6 ± 0.2	66.5 ± 0.5	9.9 ± 0.1	9.99
0.75:0.25:1.1	300	0.761 ± 0.002	19.5 ± 0.2	65.7 ± 0.6	9.7 ± 0.1	9.83
0.75:0.25:1.1	400	0.754 ± 0.005	19.8 ± 0.2	55.6 ± 0.1	8.3 ± 0.1	8.37
0:1:1.1	250	0.886 ± 0.003	13.8 ± 0.1 (13.21)	74.8 ± 1.2	9.2 ± 0.1	9.21
0.75:0.25:1.1[c]	250	0.751 ± 0.004	21.4 ± 0.2 (20.49)	70.0 ± 0.4	11.3 ± 0.1	11.40

[a]Statistical data obtained from 10 independent devices. [b]The J_{SC} calculated from the EQE spectrum. [c]Use of an inverted device structure.

Here, we report a highly efficient thick-film ternary OSC via the introduction of a nematic liquid crystalline small molecule benzodithiophene terthiophene rhodanine (BTR)[44] into a host binary system of poly[4,8-bis(5-(2-ethylhexyl)thiophen-2-yl)-benzo[1,2-*b*:4,5-*b*′]dithiophene-*co*-3-fluorothieno[3,4-*b*]-thiophene-2-carboxylate] (PTB7-Th):[6,6]-phenyl C71 butyric acid methyl ester (PC71BM). The chemical structures and energy levels of PTB7-Th (M_n = 85k, M_w = 263k, and PDI = 3.1), BTR, and PC71BM are shown in Figure 1a,b. PTB7-Th was selected because of its high device PCE when blended with PC71BM.[17−19] However, the optimal active layer thickness of PTB7-Th:PC71BM devices was limited to approximately 100 nm, mainly due to the relatively low hole mobility of PTB7-Th, which would cause poor charge extraction and severe charge recombination in thick-film BHJ devices.[51−53] Therefore, the high crystallinity small molecule BTR was chosen as the third component with the expectation of increasing the mobility of the PTB7-Th:PC71BM system. It was determined experimentally that the addition of BTR into the PTB7-Th:PC71BM system can decrease the $\pi-\pi$ stacking distance, enlarge the coherence length, and enhance the domain purity of the blend film, thus significantly increasing the hole mobility of the ternary active layer. This allowed the optimal active layer thickness of the ternary OSCs to be increased to 250 nm. In addition, the absorption of PTB7-Th was complemented by BTR in the short wavelength region from 400 to 620 nm (Figure 1c), thus broadening the absorption in the visible range (300 to 800 nm) in the ternary blend films (Figure S1b). As a result, significant enhancement of light harvesting was achieved. With a conventional device structure, PCEs were drastically improved from 7.07% (active layer thickness ∼250 nm) and 9.03% (∼100 nm) to 10.37% (∼250 nm) and 10.16% (∼100 nm), respectively, by the addition of 25% (w/w) BTR into PTB7-Th:PC71BM. Furthermore, when using an inverted device structure, the PCE of the optimized ternary system was improved to 11.40% (∼250 nm), which is, to the best of our knowledge, one of the highest-efficiency ternary OSCs reported to date. Unlike most reported high-performance (PCE > 10%) OSCs with a thick active layer processed by hot spin-coating,[7,9,10,54] this ternary system is the first reported high-performance OSC with a thick active layer that can be processed at room temperature and that can meet the needs of future roll-to-roll production.

RESULTS AND DISCUSSION

Device Performance of OSCs. To investigate the effects of introducing BTR into the PTB7-Th:PC71BM system, a conventional device with a device structure of indium tin oxide (ITO)/PEDOT:PSS/PTB7-Th:BTR:PC71BM/PFNBr/Ag was used. The weight ratio of donors to PC71BM was kept at 1:1.1 in this study. First, the active layer thickness was fixed at about 100 nm. The photovoltaic performances of the binary and ternary OSCs under AM 1.5 G illumination at 100 mW/cm^2 are summarized in Table 1 and Figure 2a. It is worth mentioning that the optimized volume fraction of 1,8-diiodooctane (DIO) can be reduced from 3% (reported by most works based on PTB7-Th:PC71BM)[17,18,34] to 0.5% (Table S1) in ternary systems. Devices based on PTB7-Th:PC71BM with both 0.5% and 3% DIO exhibited comparable performance. However, to maintain a consistent experimental condition with the ternary device, we mainly investigate and discuss the device with 0.5% DIO. The PTB7-Th:PC71BM control devices with 0.5% DIO exhibited a best PCE of 9.03% with a J_{SC} of 16.87 mA cm^{-2}, an open-circuit voltage (V_{OC}) of 0.782 V, and an FF of 68.54%. Meanwhile, the BTR:PC71BM devices showed a best PCE of 6.97% with a J_{SC} of 10.67 mA cm^{-2}, a V_{OC} of 0.886 V, and an FF of 73.94%. For a ternary system with 10%, 20%, and 25% of BTR, the FF was significantly enhanced from 68.54% to 73.76%, 75.42%, and 75.96%, respectively. The J_{SC} increased slightly from 16.87 mA cm^{-2} to 17.44 mA cm^{-2}, 17.16 mA cm^{-2}, and 17.08 mA cm^{-2}, respectively. With the V_{OC} pinned at ∼0.78 V, the PCEs increased significantly from 9.03% to 10.09%, 10.15%, and 10.16%, respectively. When the BTR content was raised to 30%, although the FF was still maintained at 75.56%, the J_{SC} and V_{OC} slightly decreased to 16.87 mA cm^{-2} and 0.775 V, respectively, resulting in a final PCE of 9.75%. It is worth noting that the V_{OC} values of the ternary OSCs were pinned to the smaller V_{OC} of the PTB7-Th:PC71BM binary system at various BTR contents, which may be attributed to the fact that the V_{OC} of OSCs is mainly determined by the smallest difference between the HOMO energy levels of donor materials and the LUMO energy levels of acceptor materials, as reported elsewhere.[37,55,56] This differs from the observation reported in some studies that the V_{OC} of the ternary OSCs was located between the V_{OC} of two binary OSCs due to the formation of organic alloys,[34,57] cocrystals,[58] or a parallel-like BHJ.[59,60] Therefore, in this study, the introduction of BTR into PTB7-

DOI: 10.1021/jacs.6b11991
J. Am. Chem. Soc. 2017, 139, 2387−2395

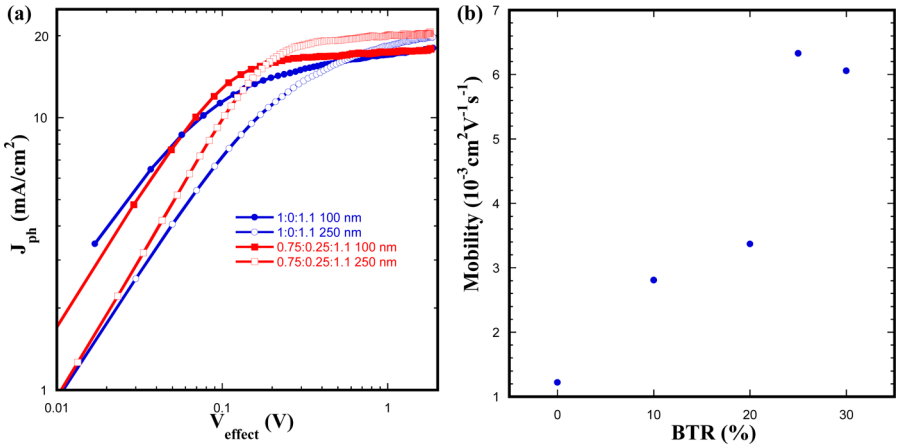

Figure 3. (a) Photocurrent density (J_{ph}) versus effective voltage (V_{effect}) curves of OSCs with PTB7-Th:BTR:PC71BM ratios of 1:0:1.1 and 0.75:0.25:1.1 with thin and thick active layers. (b) SCLC hole mobility (~100 nm films) versus various contents of BTR.

Th:PC71BM may not form an alloy or cocrystals but may only improve the morphology of the active layer.

To further study the possible effect of improving charge transportation by incorporating BTR and to verify our expectation of achieving a thick film device, optimized ternary OSCs (25% BTR) with active layer thicknesses from 100 to 400 nm were fabricated. The results are summarized in Table 2 and Figure 2b. From Table 2, it can be found that the optimal active layer thickness of ternary OSCs is about 250 nm. When the thickness of the active layer was increased to 250 nm, although the FF decreased from 75.96% (active layer thickness of 100 nm) to 68.21% and the V_{OC} slightly decreased from 0.782 to 0.763 V (the same phenomenon was reported in some studies of a thick active layer),[22,44] the J_{SC} significantly increased from 17.08 mA cm^{-2} to 19.92 mA cm^{-2}, thus resulting in a higher PCE of 10.37%. As the thickness of the active layers was further increased to 300 and 400 nm, the J_{SC} slightly decreased to 19.67 mA cm^{-2} and 19.87 mA cm^{-2}, respectively, and the FF also decreased to 65.63% and 55.63%, resulting in an acceptable drop in PCE of 9.83% and 8.37%, respectively. For control devices, PTB7-Th:PC71BM devices with a 250 nm-thick active layer showed a slight enhancement in J_{SC} but a dramatic drop in FF to 50.90% compared with the thin active layer devices, resulting in a poor PCE of 7.07%. When the thickness of active layers was further increased to 400 nm, the J_{SC} and FF dramatically decreased to 12.73 mA cm^{-2} and 41.52%, respectively, resulting in a very poor PCE of 4.03%. The BTR:PC71BM device with a 250 nm-thick active layer showed better performance than its comparable thin active layer device and exhibited a PCE of 9.21%, which was comparable with the data reported in the literature.[44] To summarize, by introducing 25% BTR into the PTB7-Th:PC71BM binary system, efficient ternary OSCs with an optimal active layer thickness of 250 nm were achieved, resulting in improvement of the PCE by 14.8% and 46.7% compared with PTB7-Th:PC71BM binary OSCs with 100 and 250 nm active layers, respectively. The performance of the optimized ternary OSCs was further improved when an inverted device structure[7] was used (ITO/ZnO/PTB7-Th:BTR:PC71BM/MoO_3/Ag) with a best PCE of 11.40% (J_{SC} = 21.66 mA cm^{-2}, V_{OC} = 0.745 V, and FF = 70.6%). The external quantum efficiency (EQE) curves of the binary and ternary OSCs are shown in Figures 2d and S2b. The J_{SC} values calculated from the EQE curves are also shown in Tables 1 and 2, and these values were consistent with the measured J_{SC} values indicating an error of about or <5%. For devices with 100 nm active layers, the EQE values were enhanced in the region from 450 to 600 nm with incorporation of BTR, were slightly decreased in the region from 620 to 720 nm, and were consistent with the absorption spectra (Figure S1b). Therefore, compared to thin-film PTB7-Th:PC71BM binary system, it only resulted in a slight enhancement in J_{SC} for thin-film ternary systems, which can also be found in other reported ternary systems.[31,34,42] When the thickness of the active layers was increased to 250 nm, the EQE values for the ternary devices showed significant increase over the whole wavelength range. The large increase of EQE from 400 to 600 nm can be mainly attributed to the complementary absorption of BTR. The relatively small increase of EQE from 650 to 750 nm should be attributed to thicker PTB7-Th. This suggests that both PTB7-Th and BTR worked independently with PC71BM in ternary devices and both contributed to the photocurrent.[55,59] The internal quantum efficiency (IQE) were measured to investigate how efficient the devices were converting absorbed photons into collected charges. In Figure S2c, IQE values of thin-film (100 nm) ternary devices (25% BTR) were slightly higher than thin-film (100 nm) PTB7-Th:PC71BM binary devices in the region from 350 to 600 nm, which can be attributed to the charge generation from the BTR:PC71BM "sub-cell". When the thickness of PTB7-Th:PC71BM binary film was increased to 250 nm, the IQE values decrease in the range of 500 to 750 nm, which may be attributed to more bimolecular recombination and less charge collection in thick-film devices. While in the ternary system (25% BTR), when the thickness was increased to 250 nm, the IQE values remain about the same in the long wavelength region and show a slight increase in the short wavelength region, which can be attributed the fact that BTR can work well in thick-film devices. These data show that thick-film ternary OSCs are even more efficient to convert absorbed photons into collected charges than thin-film ternary OSCs. In addition, the thick active layer can absorb more photons, and these factors combined led to a much higher J_{SC} in thick-film ternary OSCs.

Charge Generation, Separation, and Transport Properties. To gain more insight into the light absorption and exciton dissociation processes, saturation current density (J_{sat}) measurement and charge dissociation probabilities P(E, T) analysis of the binary and ternary OSCs were carried out.

DOI: 10.1021/jacs.6b11991
J. Am. Chem. Soc. 2017, 139, 2387−2395

Figures 3a and S2d present curves of photocurrent density (J_{ph}) versus effective voltage (V_{eff}) of the OSCs used in this study. J_{ph} is defined as $J_{ph} = J_L - J_D$, where J_L and J_D are the light and dark current density, respectively. V_{eff} is defined as $V_{eff} = V_o - V_a$, where V_o is the voltage when J_{ph} is equal to zero, and V_a is the applied bias voltage.[37] It is assumed that all of the photogenerated excitons were dissociated into free charges and collected by electrodes at high V_{eff} (in this case, about 1.8 V). Therefore, the J_{sat} will only be limited by the total amount of absorbed incident photons. The J_{sat} values for PTB7-Th:PC71BM binary devices and ternary devices were 17.88 mA cm^{-2} (0% BTR, 100 nm), 19.73 mA cm^{-2} (0% BTR, 250 nm), 18.10 mA cm^{-2} (10% BTR, 100 nm), 17.78 mA cm^{-2} (20% BTR, 100 nm), 17.77 mA cm^{-2} (25% BTR, 100 nm), 20.42 mA cm^{-2} (25% BTR, 250 nm), and 17.10 mA cm^{-2} (30% of BTR, 100 nm), respectively. With the 100 nm active layer, there was only slight enhancement of J_{sat} when 10% BTR was incorporated into the PTB7-Th:PC71BM binary system, and further increase of the BTR content led to a decrease in J_{sat}. However, the J_{sat} of the ternary system (25% BTR) was significantly enhanced when the active layer become thick (250 nm) and was 14.2% higher than that of the thin films in the PTB7-Th:PC71BM binary system. This result proved our original purpose of using a thick ternary blend film to greatly enhance light harvesting to improve the J_{SC} of the ternary OSCs. However, the J_{SC} for the optimized ternary system (25% BTR) with thick active layer was enhanced by 18.1% compared with that in the PTB7-Th:PC71BM binary system with thin film, which was much higher than the J_{sat} enhancement of 14.2%, indicating different P(E, T) for these devices. P(E, T) is determined by normalizing J_{ph} with J_{sat} (J_{ph}/J_{sat}). Under the short-circuit condition, the P(E, T) values are 96.6%, 97.2%, 96.8%, and 97.4% for ternary OSCs (active layer thickness of about 100 nm) with 10%, 20%, 25%, and 30% BTR, respectively. These values were higher than that of PTB7-Th:PC71BM binary OSCs (94.3%, active layer thickness of about 100 nm), indicating that the incorporation of BTR into PTB7-Th:PC71BM was beneficial for the charge dissociation process. Furthermore, the ternary OSCs (25% BTR, 250 nm) still maintained a high P(E, T) of 97.8%, whereas the P(E, T) of the PTB7-Th:PC71BM binary OSCs (250 nm) decreased to 89.3%. This result showed that the incorporation of BTR helped to achieve efficient ternary OSCs with a thick active layer by increasing light absorption and facilitating charge dissociation. Figure S2e shows the PL emission spectra of pure BTR and PTB7-Th films along with BTR:PTB7-Th blends of different ratios. These PL emission results show that there is negligible PL emissions from BTR for all the BTR:PTB7-Th blends, while the increase of BTR weight ratio in the blends led to a significant increase of the PL emission from PTB7-Th. This result indicates that there is efficient energy transfer occurring from BTR to PTB7-Th. For the ternary blends, the excitons generated on BTR have two possible pathways to generate charges. One is direct electron transfer to PC71BM, and the other is energy transfer to PTB7-Th and then electron transfer to PC71BM.

Because it was already reported that high mobility of the charge carriers is required for high FF in BHJ OSCs, especially for thick film devices,[52] the hole mobility of the binary and ternary blend films was measured by using the space-charge-limited current method with device structure ITO/PEDOT:PSS/binary or ternary blend films/MoO_3/Ag to further investigate the reason for the efficiency of these thick film ternary OSCs. The results are summarized in Figures S3 and 3b and Table S2. The hole mobility in PTB7-Th:PC71BM and BTR:PC71BM binary blend films with a thickness around 100 nm was 1.22×10^{-3} cm^2 V^{-1} s^{-1} and 1.48×10^{-3} cm^2 V^{-1} s^{-1}, respectively (comparable to the values reported in other studies).[34,44,55] When BTR was introduced into PTB7-Th:PC71BM, the hole mobility significantly increased to a very high value of 6.33×10^{-3} cm^2 V^{-1} s^{-1} with 25% BTR. The increased hole mobility may contribute to the increased FF obtained in the ternary OSCs. When the content of BTR was further increased to 30%, the hole mobility decreased slightly to 6.06×10^{-3} cm^2 V^{-1} s^{-1}. It has been noted that the hole mobility of the ternary blend films was higher than that in both binary blend films, as was also reported previously.[31,34,36] We attributed this phenomenon to the improvement in morphology achieved by adding the highly crystalline small molecule BTR into PTB7-Th:PC71BM. Moreover, it should be noted that the PTB7-Th:PC71BM binary and ternary blend films were prepared from chlorobenzene solutions, whereas the BTR:PC71BM blend films were prepared from chloroform solutions to impede overcrystallization of the BTR to obtain a good film with fine phase separation size, just like that reported in other small molecular systems.[8,61,62] Therefore, blending of BTR into PTB7-Th:PC71BM and fabrication from a chlorobenzene solution can facilitate the BTR molecules to arrange themselves well but not to overcrystallize. This may be the reason why the high crystallinity BTR blended with PC71BM exhibited a lower hole mobility than the ternary film. Furthermore, the mobility of these two binary and ternary blend films (25% BTR) with thickness of 240 to 250 nm was also measured. A slight decrease in hole mobility from 6.33×10^{-3} to 5.01×10^{-3} cm^2 V^{-1} s^{-1} was observed as the thickness increased from 100 to 240 nm in the ternary blend films, but almost no decrease was found in the BTR:PC71BM binary blend films when the thickness increased from 140 to 250 nm, as the hole mobility was maintained at 1.41×10^{-3} cm^2 V^{-1} s^{-1}. However, in the case of the PTB7-Th:PC71BM binary blend films, the hole mobility decreased more from 1.22×10^{-3} to 8.86×10^{-4} cm^2 V^{-1} s^{-1}. These results supported the variation in FF of the OSCs mentioned above because the charge with higher mobility will transport to the electrode more quickly, thus reducing charge recombination[52] and enhancing charge extraction. This is also one reason that ternary OSCs and BTR:PC71BM binary OSCs with a thicker active layer film (250 nm) can achieve a higher PCE than the thinner ones, but the PTB7-Th:PC71BM binary OSCs with thicker active layer film had a worse PCE than the thinner ones.

Furthermore, a similar small molecule (DR3TSBDT) (Figure S4) with lower hole mobility (~10^{-4} cm^2 V^{-1} s^{-1}) and thinner optimal active layer thickness in OSCs (~110 nm)[62] was used to replace BTR. The device (conventional structure) results show that DR3TSBDT did not work as well as BTR in thick-film ternary OSCs (Table S3). These results suggest that the high hole mobility of liquid crystalline small molecule BTR[44] is the main factor that enables the efficient thick-film ternary OSCs.

Charge Recombination and Extraction Dynamics. In addition to light absorption, exciton dissociation, and charge transportation, the dependence of J_{SC} at various light intensities was also measured to investigate the recombination process in the PTB7-Th:PC71BM binary and ternary devices. Quantitatively, J_{SC} follows a power-law dependence on light intensity ($J_{SC} \propto P_{light}^{S}$), where P_{light} is light intensity and S is the

DOI: 10.1021/jacs.6b11991
J. Am. Chem. Soc. 2017, 139, 2387−2395

exponential factor.[63,64] Generally, weak bimolecular recombination is suggested when J_{SC} shows a linear dependence on P_{light} with the S value close to 1. As shown in Figures S5 and 4a, the S values were very close to 1 for all devices with a thin active layer, indicating that the bimolecular recombination was very weak in these devices. However, the S values of the binary devices decreased to 0.971 when the active layer thickness increased to 250 nm, but for the ternary devices, the S value decreased only slightly to 0.995. This result is easy to understand because in a low charge mobility system, it takes a long time for charges to transport to electrodes, which increases the possibility of recombination. However, in the case of a high charge mobility system, such recombination is largely reduced.[52]

The charge extraction process was investigated by using transient photocurrent measurements. As shown in Figure 4b,

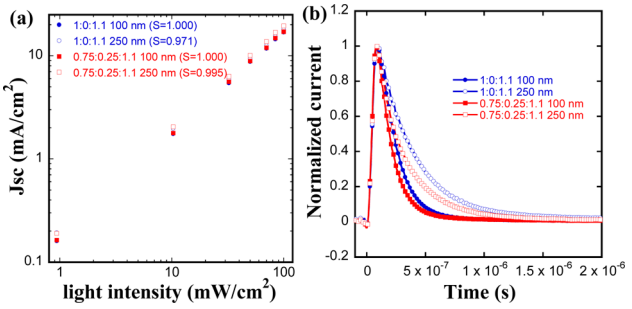

Figure 4. (a) Short-circuit density (J_{SC}) versus light intensity (P_{light}) and (b) transient photocurrent of OSCs with PTB7-Th:BTR:PC71BM ratios of 1:0:1.1 and 0.75:0.25:1.1 with thin and thick active layers.

the ternary devices (25% BTR) had a shorter charge extraction time (0.14 μs) than the PTB7-Th:PC71BM binary devices (0.17 μs) when the active layer thickness was about 100 nm. As the active layer thickness increased to 250 nm, the charge extraction time of the binary and ternary devices also increased. However, the ternary devices still had a shorter charge extraction time (0.23 μs) than that of the binary devices (0.31 μs). This result was consistent with the mobility values discussed above in that higher mobility resulted in a shorter charge extraction time for the same active layer thickness. The charge extraction time will increase as the active layer thickness increases. The introduction of BTR into PTB7-Th:PC71BM can increase the charge extraction rate and thus reduce charge recombination, which is the major reason for higher the FF and PCE in ternary devices.

Morphology Characterization. To study the influence of BTR on the morphology of the films of the ternary blends, atomic force microscopy (AFM) measurements and transmission electron microscopy (TEM) were performed. As shown in Figures 5 and S6, the thin PTB7-Th:PC71BM film (100 nm) exhibited uniform morphology and a smooth surface with a root-mean-square (RMS) roughness value of 0.91 nm, whereas the thick PTB7-Th:PC71BM film (250 nm) showed a rougher surface with a RMS value of 1.34 nm, possibly due to phase aggregation. After adding 10%, 20%, and 25% BTR, the ternary blend films still maintained a uniform morphology and smooth surface with similar RMS values of 0.93, 1.09, and 0.93 nm, respectively. This may have resulted from the good miscibility between PTB7 and BTR, as they both have a benzodithiophene (BDT) unit in their molecule structures.

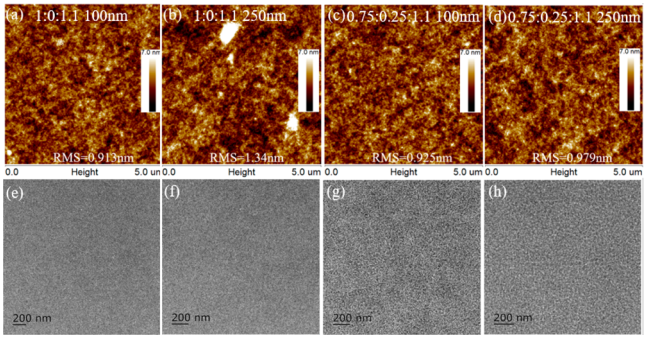

Figure 5. (a–d) AFM height images and (e–h) TEM images for PTB7-Th:BTR:PC71BM blend films with various BTR content and specific thickness: (a, e) 1:0:1.1 100 nm; (b, f) 1:0:1.1 250 nm; (c, g) 0.75:0.25:1.1 100 nm; and (d, h) 0.75:0.25:1.1 250 nm.

When the thickness of the ternary blend film with 25% BTR was increased to 250 nm, the RMS value slightly increased to 0.98 nm but remained at the same level as the above-mentioned ternary blend films. However, when the BTR content increased to 30%, the ternary blend film showed a very rough surface with obvious phase aggregation, and the RMS value increased significantly to 3.13 nm due to the high crystallinity of the BTR, which may be the main reason for the lower J_{SC} and PCE of the resulting devices. From the TEM images, the ternary blend films showed more obvious and better phase separation than the PTB7-Th:PC71BM films, which can be beneficial for excitons separation and charge transportation. Furthermore, fine dispersed fibrils could be clearly observed in the ternary blend films when the content of BTR was increased to 25% and 30% (as also found in the BTR:PC71BM film), which provided more high-speed channels for charge transportation.

Grazing incidence wide-angle X-ray scattering (GIWAXS) was used to investigate the crystallinity and molecular packing in the blend films with various BTR content. Figure 6a–f displays the GIWAXS two-dimensional (2D) patterns of blend films of two referential binary systems and ternary systems with different additions of BTR up to 30% (corresponding 1D line-cuts in the in-plane and out-of-plane directions are shown in Figure 6g). In general, broad (100) lamellar peaks of PTB7-Th at 0.30 Å^{-1} are observed in the binary and ternary systems, and there was little change in peak location and intensity with the addition of BTR except for a sharp (100) peak of BTR at 0.33 Å^{-1} appearing when 30% BTR was added to the blend. This tendency indicates that the addition of BTR to the system did not improve the lamellar packing much. Nevertheless, the BTR has a more noticeable influence on $\pi-\pi$ stacking. The PC71BM diffraction peak is located at q values of about 1.32 Å^{-1} with significant intensity in both the out-of-plane and in-plane directions. The fitting patterns of 1D line cuts in the out-of-plane direction is shown in Figure 6a′–f′, and the related crystallinity parameters are summarized in Table 3. As BTR was gradually added to the optimal ratio (25%), the PTB7-Th (010) peak relating to $\pi-\pi$ stacking in the out-of-plane direction shifts to a higher q from 1.53 Å^{-1} to 1.67 Å^{-1} and then shifts back with the addition of more BTR; in other words, the blend film with 25% BTR has the most compact $\pi-\pi$ stacking with d-spacing of around 3.77 Å. This result corresponds well to the slight bathochromic shift of absorption peaks in the long wavelength observed in the absorption spectra. Furthermore, the coherence lengths (Table 3) of the binary blends and ternary blends with various contents were

DOI: 10.1021/jacs.6b11991
J. Am. Chem. Soc. 2017, 139, 2387–2395

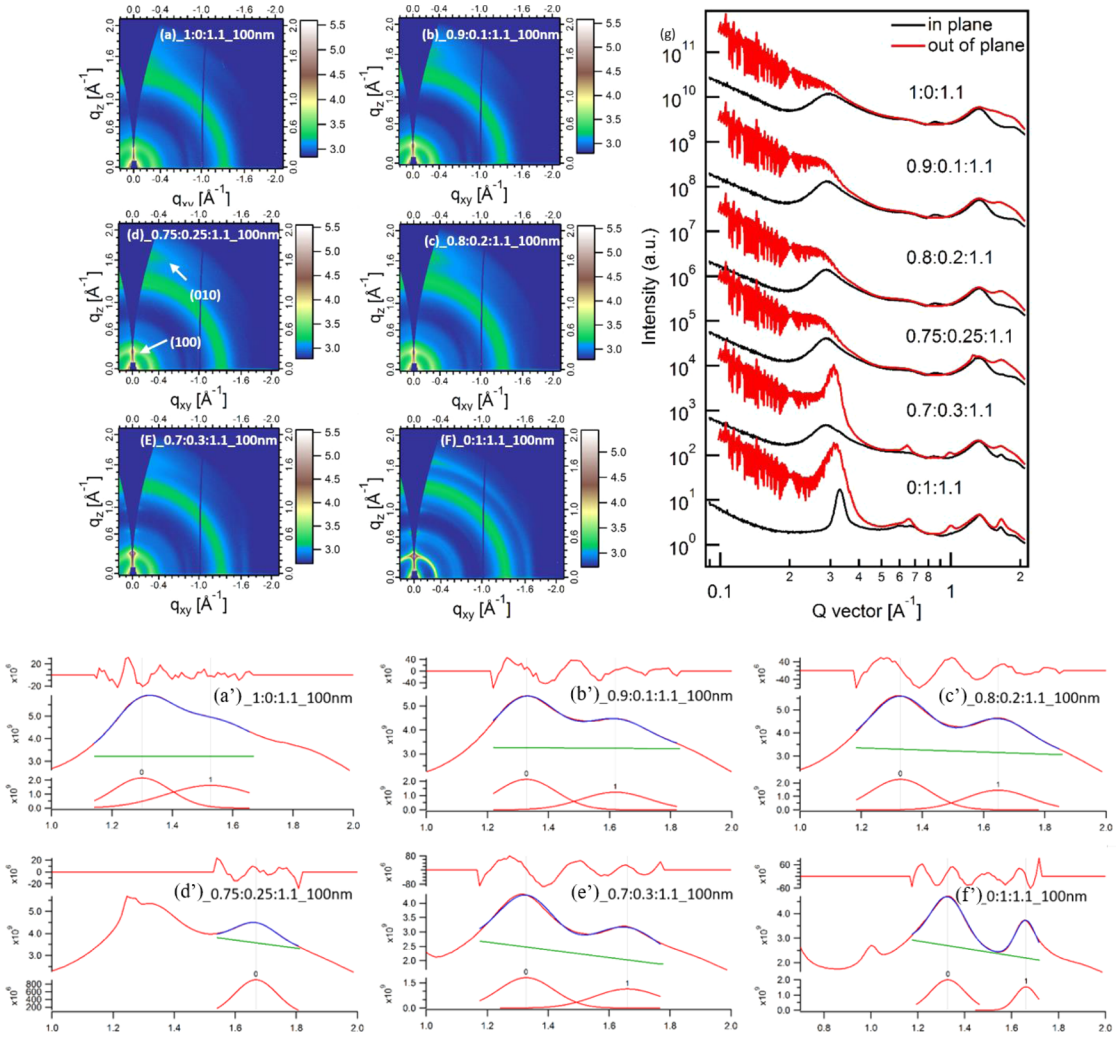

Figure 6. (a–f) GIWAXS 2D patterns for PTB7-Th:BTR:PC71BM blend films with various contents of BTR and 100 nm thickness, (g) 1D line-cuts, and (a′–f′) the fitting patterns of 1D line cuts in the out-of-plane direction.

Table 3. Related Data of GIWAXS and R-SoXS Characterization for Various Ratios of PTB7-Th:BTR:PC$_{71}$BM 100 nm Active Layer Films

PTB7-Th:BTR:PC$_{71}$BM	$\pi-\pi$ stacking peak location (Å^{-1})	d-spacing (Å)	coherence length (Å)	domain purity
1:0:1.1	1.53	4.11	16.51	0.53
0.9:0.1:1.1	1.62	3.88	21.52	0.69
0.8:0.2:1.1	1.65	3.81	22.59	0.70
0.75:0.25:1.1	1.67	3.77	34.78	0.75
0.7:0.3:1.1	1.66	3.78	22.16	0.72
0:1:1.1	1.66	3.78	53.34	1

estimated by the Scherrer equation.[65] Among the ternary systems, the ternary blend film with 25% BTR showed the largest coherence length of 34.8 Å, and it was also better than that for the PTB7-Th:PC71BM binary system.

The decreased $\pi-\pi$ stacking distance (d-spacing) and enlarged coherence length are beneficial to charge transport and the mitigation of bimolecular recombination,[34,66] which correlate well with the hole mobility results discussed above. Thus, the highest FF was obtained at the optimal BTR content.

Resonant soft X-ray scattering (R-SoXS) was also carried out to detect the domain size (characteristic phase separation length scale) and relative average domain purity of the blend films. Lorentz-corrected R-SoXS scattering profiles of different BTR content blend films are shown in Figure 7. Log-normal distribution fitting results (Figure S7) reveal that the PTB7-Th:PC71BM binary and ternary blends with various BTR content show a similar hierarchical morphology on three length scales. The similar domain size can explain the small differences

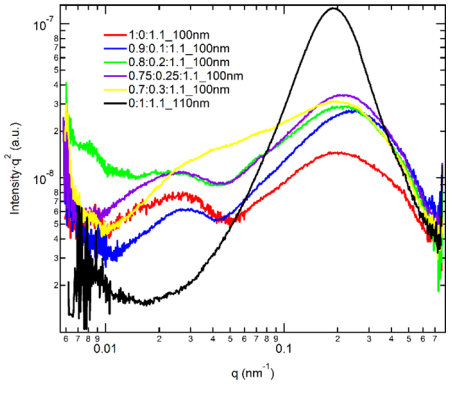

Figure 7. R-SoXS scattering profiles of PTB7-Th:BTR:PC71BM blend films with various content of BTR with 100 nm thickness.

DOI: 10.1021/jacs.6b11991
J. Am. Chem. Soc. 2017, 139, 2387–2395

of J_{SC} between different ternary blend systems, as domain size has a large effect on J_{SC}.[67] Although the addition of BTR leads to little change on the characteristic phase separation length scale, the domain purity varies considerably. The relative average domain purity (shown in Table 3) is estimated by calculating the total scattering intensity through the integration of the scattering profiles over the q range and taking film thickness into account.[67] The blend film of 25% BTR obtained the highest domain purity among the ternary systems and was also higher than the PTB7-Th:PC71BM binary system, which could be another reason for its high mobility and FF.

It has been reported that some nucleating agents[68,69] can induce the crystallization of conventional polymers such as polypropylene. We speculate that BTR may play a similar role as a nucleating agent to induce the arrangement, orientation, or even crystallization of PTB7-Th, which result in decreased $\pi-\pi$ stacking distance, enlarged coherence length, and enhanced domain purity in blend film. It can also be clearly observed in TEM images that fine dispersed fibrils were produced when 25% of BTR is added into the PTB7-Th:PC71BM blend, which may indicate the formation of more ordered polymer domains

Furthermore, BTR was introduced into a non-BDT polymer system poly[*N*-9′-heptadecanyl-2,7-carbazole-*alt*-5,5-(4′,7′-di-2-thienyl-2′,1′,3′-benzothiadiazole)] (PCDTBT)[70] (Figure S8) to explore the general applicability of our approach. The device (conventional structure) results (Table S4) show that both thin-film (80 nm) and thick-film (250 nm) PCDTBT:BTR:PC71BM ternary OSCs exhibited a higher PCE than thin-film (80 nm) and thick-film (250 nm) PCDTBT:PC71BM binary OSCs, respectively. Due to the low hole mobility of PCDTBT (~10^{-5} cm^2 V^{-1} s^{-1} to 10^{-4} cm^2 V^{-1} s^{-1}),[71] when the thickness of PCDTBT:PC71BM binary film increased from 80 to 250 nm, the devices' PCE dropped a lot, which only remain 66.6% of that with 80 nm. However, the introduction of BTR mitigated the PCE loss caused by the increased thickness, and the PCE still remained at 86.6% when the thickness of PCDTBT:BTR:PC71BM ternary film increased from 80 to 250 nm. Therefore, our approach is not only applicable to BDT polymer system but also non-BDT polymer system, which may have wide applications in ternary OSCs.

CONCLUSION

We have successfully developed a highly efficient ternary OSC with thick active layer by introducing the highly crystalline small molecule BTR into a PTB7-Th:PC71BM host blend. This OSC could be a potential candidate for future roll-to-roll mass production because of its thickness-insensitive performance and ability to be processed at room temperature. Compared with binary systems, a higher PCE of 10.37% was achieved for ternary OSCs with 25% (w/w) BTR content at the 250 nm-thick active layer, mainly because of improved light harvesting, more efficient charge separation, faster charge transport, more efficient charge extraction resulting from higher mobility, and optimized BHJ morphology. The PCE of the optimized ternary OSCs was further improved to 11.40% when using an inverted device structure. Therefore, our results showed that the introduction of a highly crystalline small molecular material into ternary OSCs is an efficient way to achieve high-performance thick-film devices that can meet the needs of future roll-to-roll production.

ASSOCIATED CONTENT

Supporting Information

The Supporting Information is available free of charge on the ACS Publications website at DOI: 10.1021/jacs.6b11991.

Complete experimental section, cyclic voltammograms, photoluminescent spectra, IQE spectra, additional UV–vis absorption spectra, SCLC data, atomic force microscopy, transmission electron microscopy images, and R-SoX 1D line fitting patterns (PDF)

AUTHOR INFORMATION

Corresponding Author

*msfhuang@scut.edu.cn

ORCID

Fei Huang: 0000-0001-9665-6642

Notes

The authors declare no competing financial interest.

ACKNOWLEDGMENTS

This work was financially supported by the Ministry of Science and Technology (no. 2014CB643501) and the Natural Science Foundation of China (nos. 21520102006, 51521002, 91633301 and 51361165301). X-ray data was acquired at beamlines 7.3.3 and 11.0.1.2 at the Advanced Light Source, which is supported by the Director, Office of Science, Office of Basic Energy Sciences, of the U.S. Department of Energy under Contract no. DE-AC02-05CH11231. W.M., Z.W., and J.X. are thankful for the support received from the Natural Science Foundation of China (nos. 21504066 and 21534003), and they thank Chenhui Zhu at beamline 7.3.3, and Cheng Wang at beamline 11.0.1.2 for their assistance with data acquisition. H.Y. thanks the Hong Kong Innovation and Technology Commission for support received through ITC-CNERC14SC01.

REFERENCES

(1) Cheng, Y.-J.; Yang, S.-H.; Hsu, C.-S. *Chem. Rev.* **2009**, *109*, 5868.
(2) Scharber, M. C.; Sariciftci, N. S. *Prog. Polym. Sci.* **2013**, *38*, 1929.
(3) Huang, Y.; Kramer, E. J.; Heeger, A. J.; Bazan, G. C. *Chem. Rev.* **2014**, *114*, 7006.
(4) Lu, L.; Zheng, T.; Wu, Q.; Schneider, A. M.; Zhao, D.; Yu, L. *Chem. Rev.* **2015**, *115*, 12666.
(5) Mazzio, K. A.; Luscombe, C. K. *Chem. Soc. Rev.* **2015**, *44*, 78.
(6) van der Poll, T. S.; Love, J. A.; Nguyen, T.-Q.; Bazan, G. C. *Adv. Mater.* **2012**, *24*, 3646.
(7) Liu, Y.; Zhao, J.; Li, Z.; Mu, C.; Ma, W.; Hu, H.; Jiang, K.; Lin, H.; Ade, H.; Yan, H. *Nat. Commun.* **2014**, *5*, 5293.
(8) Kan, B.; Li, M.; Zhang, Q.; Liu, F.; Wan, X.; Wang, Y.; Ni, W.; Long, G.; Yang, X.; Feng, H.; Zuo, Y.; Zhang, M.; Huang, F.; Cao, Y.; Russell, T. P.; Chen, Y. *J. Am. Chem. Soc.* **2015**, *137*, 3886.
(9) Vohra, V.; Kawashima, K.; Kakara, T.; Koganezawa, T.; Osaka, I.; Takimiya, K.; Murata, H. *Nat. Photonics* **2015**, *9*, 403.
(10) Zhao, J.; Li, Y.; Yang, G.; Jiang, K.; Lin, H.; Ade, H.; Ma, W.; Yan, H. *Nat. Energy* **2016**, *1*, 15027.
(11) Jin, Y.; Chen, Z.; Dong, S.; Zheng, N.; Ying, L.; Jiang, X.-F.; Liu, F.; Huang, F.; Cao, Y. *Adv. Mater.* **2016**, *28*, 9811.
(12) Li, Y. *Acc. Chem. Res.* **2012**, *45*, 723.
(13) Lin, Y.; Wang, J.; Zhang, Z.-G.; Bai, H.; Li, Y.; Zhu, D.; Zhan, X. *Adv. Mater.* **2015**, *27*, 1170.
(14) Gao, L.; Zhang, Z.-G.; Xue, L.; Min, J.; Zhang, J.; Wei, Z.; Li, Y. *Adv. Mater.* **2016**, *28*, 1884.
(15) Yang, Y.; Zhang, Z.-G.; Bin, H.; Chen, S.; Gao, L.; Xue, L.; Yang, C.; Li, Y. *J. Am. Chem. Soc.* **2016**, *138*, 15011.
(16) Li, S.; Ye, L.; Zhao, W.; Zhang, S.; Mukherjee, S.; Ade, H.; Hou, J. *Adv. Mater.* **2016**, *28*, 9423.

DOI: 10.1021/jacs.6b11991
J. Am. Chem. Soc. 2017, 139, 2387–2395

(17) Liao, S. H.; Jhuo, H. J.; Yeh, P. N.; Cheng, Y. S.; Li, Y. L.; Lee, Y. H.; Sharma, S.; Chen, S. A. *Sci. Rep.* **2014**, *4*, 6813.
(18) He, Z.; Xiao, B.; Liu, F.; Wu, H.; Yang, Y.; Xiao, S.; Wang, C.; Russell, T. P.; Cao, Y. *Nat. Photonics* **2015**, *9*, 174.
(19) Nian, L.; Zhang, W.; Zhu, N.; Liu, L.; Xie, Z.; Wu, H.; Wurthner, F.; Ma, Y. *J. Am. Chem. Soc.* **2015**, *137*, 6995.
(20) Wu, Z.; Sun, C.; Dong, S.; Jiang, X.-F.; Wu, S.; Wu, H.; Yip, H.-L.; Huang, F.; Cao, Y. *J. Am. Chem. Soc.* **2016**, *138*, 2004.
(21) Xiao, Z.; Yuan, Y.; Yang, B.; VanDerslice, J.; Chen, J.; Dyck, O.; Duscher, G.; Huang, J. *Adv. Mater.* **2014**, *26*, 3068.
(22) Huang, J.; Carpenter, J. H.; Li, C. Z.; Yu, J. S.; Ade, H.; Jen, A. K. *Adv. Mater.* **2016**, *28*, 967.
(23) You, J.; Dou, L.; Yoshimura, K.; Kato, T.; Ohya, K.; Moriarty, T.; Emery, K.; Chen, C. C.; Gao, J.; Li, G.; Yang, Y. *Nat. Commun.* **2013**, *4*, 1446.
(24) Huang, J.; Li, C. Z.; Chueh, C. C.; Liu, S. Q.; Yu, J. S.; Jen, A. K. Y. *Adv. Energy. Mater.* **2015**, *5*, 1500406.
(25) Kang, H.; Jung, S.; Jeong, S.; Kim, G.; Lee, K. *Nat. Commun.* **2015**, *6*, 6503.
(26) Zhang, K.; Gao, K.; Xia, R.; Wu, Z.; Sun, C.; Cao, J.; Qian, L.; Li, W.; Liu, S.; Huang, F.; Peng, X.; Ding, L.; Yip, H.-L.; Cao, Y. *Adv. Mater.* **2016**, *28*, 4817.
(27) Ameri, T.; Khoram, P.; Min, J.; Brabec, C. J. *Adv. Mater.* **2013**, *25*, 4245.
(28) Cheng, P.; Zhan, X. *Mater. Horiz.* **2015**, *2*, 462.
(29) Lu, L.; Kelly, M. A.; You, W.; Yu, L. *Nat. Photonics* **2015**, *9*, 491.
(30) An, Q.; Zhang, F.; Zhang, J.; Tang, W.; Deng, Z.; Hu, B. *Energy Environ. Sci.* **2016**, *9*, 281.
(31) Zhang, Y.; Deng, D.; Lu, K.; Zhang, J.; Xia, B.; Zhao, Y.; Fang, J.; Wei, Z. *Adv. Mater.* **2015**, *27*, 1071.
(32) Fang, J.; Wang, Z.; Zhang, J.; Zhang, Y.; Deng, D.; Wang, Z.; Lu, K.; Ma, W.; Wei, Z. *Adv. Sci.* **2015**, *2*, 1500250.
(33) Cheng, P.; Li, Y.; Zhan, X. *Energy Environ. Sci.* **2014**, *7*, 2005.
(34) Zhang, J.; Zhang, Y.; Fang, J.; Lu, K.; Wang, Z.; Ma, W.; Wei, Z. *J. Am. Chem. Soc.* **2015**, *137*, 8176.
(35) Cheng, P.; Yan, C.; Wu, Y.; Wang, J.; Qin, M.; An, Q.; Cao, J.; Huo, L.; Zhang, F.; Ding, L.; Sun, Y.; Ma, W.; Zhan, X. *Adv. Mater.* **2016**, *28*, 8021.
(36) Wang, Z.; Zhang, Y.; Zhang, J.; Wei, Z.; Ma, W. *Adv. Energy. Mater.* **2016**, *6*, 1502456.
(37) Lu, L.; Xu, T.; Chen, W.; Landry, E. S.; Yu, L. *Nat. Photonics* **2014**, *8*, 716.
(38) Lu, H.; Zhang, J.; Chen, J.; Liu, Q.; Gong, X.; Feng, S.; Xu, X.; Ma, W.; Bo, Z. *Adv. Mater.* **2016**, *28*, 9559.
(39) Park, K. H.; An, Y.; Jung, S.; Park, H.; Yang, C. *Energy Environ. Sci.* **2016**, *9*, 3464.
(40) Kumari, T.; Lee, S. M.; Kang, S.-H.; Chen, S.; Yang, C. *Energy Environ. Sci.* **2017**, *10*, 258.
(41) Liu, S. H.; You, P.; Li, J. H.; Li, J.; Lee, C. S.; Ong, B. S.; Surya, C.; Yan, F. *Energy Environ. Sci.* **2015**, *8*, 1463.
(42) Gasparini, N.; Jiao, X.; Heumueller, T.; Baran, D.; Matt, G. J.; Fladischer, S.; Spiecker, E.; Ade, H.; Brabec, C. J.; Ameri, T. *Nat. Energy* **2016**, *1*, 16118.
(43) Yang, Y.; Chen, W.; Dou, L.; Chang, W.-H.; Duan, H.-S.; Bob, B.; Li, G.; Yang, Y. *Nat. Photonics* **2015**, *9*, 190.
(44) Sun, K.; Xiao, Z.; Lu, S.; Zajaczkowski, W.; Pisula, W.; Hanssen, E.; White, J. M.; Williamson, R. M.; Subbiah, J.; Ouyang, J.; Holmes, A. B.; Wong, W. W.; Jones, D. J. *Nat. Commun.* **2015**, *6*, 6013.
(45) Hu, X.; Yi, C.; Wang, M.; Hsu, C.-H.; Liu, S.; Zhang, K.; Zhong, C.; Huang, F.; Gong, X.; Cao, Y. *Adv. Energy. Mater.* **2014**, *4*, 1400378.
(46) Nian, L.; Chen, Z.; Herbst, S.; Li, Q.; Yu, C.; Jiang, X.; Dong, H.; Li, F.; Liu, L.; Würthner, F.; Chen, J.; Xie, Z.; Ma, Y. *Adv. Mater.* **2016**, *28*, 7521.
(47) Price, S. C.; Stuart, A. C.; Yang, L.; Zhou, H.; You, W. *J. Am. Chem. Soc.* **2011**, *133*, 4625.
(48) Zhang, K.; Hu, Z.; Sun, C.; Wu, Z.; Huang, F.; Cao, Y. *Chem. Mater.* **2017**, *29*, 141.
(49) Duan, C.; Huang, F.; Cao, Y. *Polym. Chem.* **2015**, *6*, 8081.
(50) Savoie, B. M.; Dunaisky, S.; Marks, T. J.; Ratner, M. A. *Adv. Energy. Mater.* **2015**, *5*, 1400891.
(51) Kim, J.; Yu, K.; Kim, H.; Kwon, S.; Kim, G.; Kwon, K.; Lee, K. *Adv. Energy. Mater.* **2014**, *4*, 1301502.
(52) Bartelt, J. A.; Lam, D.; Burke, T. M.; Sweetnam, S. M.; McGehee, M. D. *Adv. Energy. Mater.* **2015**, *5*, 1500577.
(53) Kirchartz, T.; Agostinelli, T.; Campoy-Quiles, M.; Gong, W.; Nelson, J. *J. Phys. Chem. Lett.* **2012**, *3*, 3470.
(54) Kawashima, K.; Fukuhara, T.; Suda, Y.; Suzuki, Y.; Koganezawa, T.; Yoshida, H.; Ohkita, H.; Osaka, I.; Takimiya, K. *J. Am. Chem. Soc.* **2016**, *138*, 10265.
(55) Liu, T.; Huo, L.; Sun, X.; Fan, B.; Cai, Y.; Kim, T.; Kim, J. Y.; Choi, H.; Sun, Y. *Adv. Energy. Mater.* **2016**, *6*, 1502109.
(56) Khlyabich, P. P.; Rudenko, A. E.; Street, R. A.; Thompson, B. C. *ACS Appl. Mater. Interfaces* **2014**, *6*, 9913.
(57) Street, R. A.; Davies, D.; Khlyabich, P. P.; Burkhart, B.; Thompson, B. C. *J. Am. Chem. Soc.* **2013**, *135*, 986.
(58) Lu, L.; Chen, W.; Xu, T.; Yu, L. *Nat. Commun.* **2015**, *6*, 7327.
(59) Yang, L.; Zhou, H.; Price, S. C.; You, W. *J. Am. Chem. Soc.* **2012**, *134*, 5432.
(60) Lee, T. H.; Uddin, M. A.; Zhong, C.; Ko, S.-J.; Walker, B.; Kim, T.; Yoon, Y. J.; Park, S. Y.; Heeger, A. J.; Woo, H. Y.; Kim, J. Y. *Adv. Energy. Mater.* **2016**, *6*, 1600637.
(61) Zhang, Q.; Kan, B.; Liu, F.; Long, G.; Wan, X.; Chen, X.; Zuo, Y.; Ni, W.; Zhang, H.; Li, M.; Hu, Z.; Huang, F.; Cao, Y.; Liang, Z.; Zhang, M.; Russell, T. P.; Chen, Y. *Nat. Photonics* **2014**, *9*, 35.
(62) Kan, B.; Zhang, Q.; Li, M.; Wan, X.; Ni, W.; Long, G.; Wang, Y.; Yang, X.; Feng, H.; Chen, Y. *J. Am. Chem. Soc.* **2014**, *136*, 15529.
(63) Schilinsky, P.; Waldauf, C.; Brabec, C. J. *Appl. Phys. Lett.* **2002**, *81*, 3885.
(64) Riedel, I.; Parisi, J.; Dyakonov, V.; Lutsen, L.; Vanderzande, D.; Hummelen, J. C. *Adv. Funct. Mater.* **2004**, *14*, 38.
(65) Smilgies, D.-M. *J. Appl. Crystallogr.* **2013**, *46*, 286.
(66) Szarko, J. M.; Guo, J.; Liang, Y.; Lee, B.; Rolczynski, B. S.; Strzalka, J.; Xu, T.; Loser, S.; Marks, T. J.; Yu, L.; Chen, L. X. *Adv. Mater.* **2010**, *22*, 5468.
(67) Collins, B. A.; Li, Z.; Tumbleston, J. R.; Gann, E.; McNeill, C. R.; Ade, H. *Adv. Energy. Mater.* **2013**, *3*, 65.
(68) Quan, Y.; Li, H.; Yan, S. *Ind. Eng. Chem. Res.* **2013**, *52*, 4772.
(69) Fina, A.; Tabuani, D.; Frache, A.; Camino, G. *Polymer* **2005**, *46*, 7855.
(70) Blouin, N.; Michaud, A.; Leclerc, M. *Adv. Mater.* **2007**, *19*, 2295.
(71) Zhang, Y.; Zhou, H.; Seifter, J.; Ying, L.; Mikhailovsky, A.; Heeger, A. J.; Bazan, G. C.; Nguyen, T. Q. *Adv. Mater.* **2013**, *25*, 7038.

DOI: 10.1021/jacs.6b11991
J. Am. Chem. Soc. 2017, 139, 2387−2395